Complete loss of ATM function augments replication catastrophe induced by ATR inhibition and gemcitabine in pancreatic cancer models

AUTHORS

Charles R Dunlop[1], Yann Wallez[1,2], Timothy Isaac Johnson[1], Sandra Bernaldo de Quirós Fernández[1], Stephen T. Durant[2], Elaine B. Cadogan[2], Alan Lau[2], Frances M Richards[1], Duncan I Jodrell[1,3]

AFFILIATIONS

[1] Cancer Research UK Cambridge Institute, University of Cambridge, Cambridge, UK

[2] Bioscience, Early Oncology R&D, AstraZeneca, Cambridge, UK

[3] Department of Oncology, University of Cambridge, Cambridge, UK

CORRESPONDING AUTHORS

Charles.Dunlop@cruk.cam.ac.uk

dij21@cam.ac.uk

RUNNING TITLE:

ATM loss sensitises to dual AZD6738 & gemcitabine

ABSTRACT

Background: Personalised medicine strategies may improve outcomes in pancreatic ductal adenocarcinoma (PDAC), but validation of predictive biomarkers is required. Having developed a clinical trial to assess the ATR inhibitor, AZD6738, in combination with gemcitabine (ATRi/gem), we investigated ATM-loss as a predictive biomarker of response to ATRi/gem in PDAC.

Methods: Through kinase inhibition, siRNA depletion and CRISPR-knockout of ATM, we assessed how ATM-targeting affected the sensitivity of PDAC cells to ATRi/gem. Using flow cytometry, immunofluorescence and immunoblotting, we investigated how ATRi/gem synergise in ATM-proficient and ATM-deficient cells, before assessing the impact of ATM-loss on ATRi/gem sensitivity *in vivo.*

Results: Complete loss of ATM function (through pharmacological inhibition or CRISPR-knockout), but not siRNA depletion, sensitised to ATRi/gem. In ATM-deficient cells, ATRi/gem-induced replication catastrophe was augmented, while phospho-Chk2-T68 and phospho-KAP1-S824 persisted via DNA-PK activity. ATRi/gem caused growth delay in ATM-WT xenografts in NSG mice, and induced regression in ATM-KO xenografts.

Conclusions: ATM-loss augments replication catastrophe-mediated cell death induced by ATRi/gem, and may predict clinical responsiveness to this combination. ATM status should be carefully assessed in tumours from patients with PDAC, since distinction between ATM-low and ATM-null could be critical in maximising the success of clinical trials using ATM expression as a predictive biomarker.

INTRODUCTION

Pancreatic ductal adenocarcinoma (PDAC) is one of the few major cancers where overall 5-year survival remains <10% [1]. While surgical resection can be curative, the late emergence of symptoms means that most patients with PDAC have metastatic disease at presentation and are ineligible for surgery [2]. In the advanced disease setting, the combination chemotherapy regimen FOLFIRINOX (5-FU/leucovorin/irinotecan/oxaliplatin), has been shown to improve survival, but the median overall survival for patients with Stage IV disease remains <12 months [3]. This highlights the need for better therapeutic approaches. It is hoped that the rational selection of patients, through precision medicine approaches, will improve outcomes. However, for personalised treatment strategies to succeed, careful validation of potential predictive biomarkers of response is essential.

Recently, we demonstrated that the Ataxia Telangiectasia and Rad3-Related Protein (ATR) kinase inhibitor, AZD6738, synergised with gemcitabine in PDAC models [4]. A key regulator of the DNA damage response (DDR), ATR is a serine/threonine kinase which coordinates the replication stress (RS) response. Upon stalling of a replication fork, ATR acts locally to stabilise the fork, and in addition propagates a global signal throughout the nucleus by phosphorylating several targets, most notably Chk1 [5,6]. When active, Chk1 inhibits dormant origin firing to limit single stranded DNA (ssDNA)-exposure and thus prevents nuclear exhaustion of RPA [7]. Chk1 induces cell cycle arrest by phosphorylating and inhibiting CDC25 phosphatases [8,9]. This activation of the *intra-S checkpoint* allows time for attempted restart of any stalled forks and completion of DNA synthesis in the RS-affected regions. The antimetabolite gemcitabine has been used extensively in the treatment of patients with PDAC, either as a single agent or in combination with nab-paclitaxel. As a nucleoside analogue, gemcitabine impairs the replication machinery through multiple mechanisms and induces fork stalling [10], which activates the ATR/Chk1 axis. We demonstrated previously that AZD6738 prevents gemcitabine-induced intra-S checkpoint activation in PDAC cells, leading to an induction of double-strand break (DSB) markers [4]. The combination of AZD6738 and gemcitabine (ATRi/gem) inhibited growth in a panel of PDAC cell lines *in vitro*, while *in vivo* the combination induced tumour regression. As a direct result of those studies, a phase I clinical trial has been launched to assess the safety, tolerability and preliminary anti-tumour

activity of ATRi/gem in participants with advanced solid tumours, followed by an expansion phase in patients with advanced PDAC (ATRiUM; NCT03669601).

Being a novel combination, there are no established predictive biomarkers of response for ATRi/gem. Knowing that ATRi/gem induces DSBs, we hypothesised that PDAC cells deficient in DDR pathways would be hypersensitive to the combination. We focused our attention on Ataxia Telangiectasia Mutated (ATM), a DDR kinase that acts as a master regulator of cellular responses to DSBs [11,12] which is mutated or lost in a proportion of tumours of many cancer types, including in PDAC where it is a known susceptibility gene [13]. A recent comprehensive literature review of ATM deficiency in PDAC captured 5,234 pancreatic cancer patients and estimated that the prevalence of germline or somatic ATM mutations in PDAC was 6.4%, though they uncovered a large range of 1%–34% [14]. In addition, tissue microarray data-sets indicate that low ATM protein expression in PDAC occurs at around 12-17% [15,16], though there is no consensus for defining "ATM-low".

The loss of ATM in a proportion of PDAC samples, plus the central role it plays in DSB repair, make ATM a primary candidate for a potential predictive biomarker of response for ATRi/gem therapy. Loss or mutations in ATM have previously been linked, in some cancer models, to greater sensitivity to ATRi monotherapy. For example, primary CLL cells with ATM defects showed enhanced sensitivity to AZD6738 compared to wild-type or normal cells [17] and when ATM was knocked-down with siRNA in the gastric adenocarcinoma line, SNU-484, AZD6738 IC_{50} was reduced ≥ 2-fold [18]. In contrast, when Vendetti et al. used shRNAs to deplete ATM in two lung cancer lines, the shATM cells appeared more resistant to AZD6738 monotherapy than control – only when AZD6738 was combined with cisplatin did shATM sensitise [19]. In pancreatic cancer models Ayars et al. reported that MIA PaCa-2 cells treated with shATM were no more sensitive to the ATR inhibitor VX-970/VE-822 analogue, VE-821, than control cells [20]. However, work by Perkhofer et al. using mouse models of ATM-deficient PDAC suggested that ATM-loss did confer sensitivity to VE-822 [21].

This lack of consistency in the literature between cancer model, ATR inhibitor used and the experimental method of ATM depletion employed, led us to undertake an assessment of how ATM status affects ATRi sensitivity in PDAC cells, specifically using AZD6738 with and without gemcitabine, in alignment with the ATRiUM trial. By targeting ATM through multiple methods, we reveal that complete loss of ATM function - through kinase inhibition or through CRISPR

knockout, but not ATM depletion by RNA interference - sensitises to ATRi and ATRi/gem in PDAC models. We gained further insight into the mechanisms by which AZD6738 and gemcitabine synergise to induce cell death, finding evidence for replication catastrophe that was significantly augmented in ATM-deficient cells. Our results suggest that ATM status should be carefully assessed in tumours from patients with PDAC and that the distinction between ATM-low and ATM-null could be crucial in maximising the success of trials using ATM expression as a predictive biomarker.

MATERIALS AND METHODS

Cell culture and chemicals

Human cell lines were purchased from ATCC and cultured in DMEM (ThermoFisher#41966029) (MIA PaCa-2, PANC-1 and HPAF-II) or RPMI-1640 (ThermoFisher#21875034) (AsPC-1) plus 10% FBS (ThermoFisher#10270106). Murine cell lines K8484 and DT8082 were previously established from KPC mice of 129/SvJae/C57Bl/6 background in the laboratory of David Tuveson at the CRUK Cambridge Institute [22] and were grown in DMEM with 5% FBS. Lines were subjected to regular STR fingerprinting and mycoplasma tests, performed by the CRUK-CI Cell Services core facility. AZD6738, AZD0156 and AZD7648 were provided by AstraZeneca. These, plus gemcitabine hydrochloride (Tocris#3259), were dissolved in DMSO for *in vitro* experiments, kept at -20°C, and used within 3 months.

siRNA transfection

ON-TARGETplus-SMARTpool siRNAs targeting ATM were purchased from Dharmacon (#L-003201-00-0005), as well as a Non-Targeting-Control-Pool (#D-001810-10-05). Reverse transfection was achieved using Lipofectamine RNAiMax reagent (Invitrogen#13778/150), as per manufacturer's instructions. Briefly, lipofectamine-siRNA mixture was incubated in a 100mm dish, before cells were seeded on top (final siRNA concentration = 25nM). 48-hours later, cells were split and seeded for drug sensitivity assays or immunoblotting.

CRISPR/Cas9 gene editing

A previously validated all-in-one gRNA-Cas9-GFP plasmid (pAiO-WT-ATM), the human ATM-specific gRNA sequence, GTTGGTTACATACTTGGACT, cloned into the BbsI site, was kindly provided by Professor Stephen Jackson of the Wellcome Trust/CRUK Gurdon Institute, University of Cambridge, UK [23]. MIA PaCa-2 forward transfection was achieved using Lipofectamine 3000 (Invitrogen#L3000015) as per manufacturer's instructions (6-well plate). 48-hours post-transfection, cells were split and single-cell sorted (BD FACS Aria), specifically for the top 3% of GFP-positive cells, to enrich for those positively transfected. Clones were bulked up, before half of each sample was taken for genomic DNA extraction (QIAamp DNA Micro Kit #56304). From genomic DNA, the region around the sgATM-Cas9 target site was amplified by PCR and sent for Sanger nucleotide sequencing (Eurofins LightRun). Sequencing chromatograms were deconvoluted using the Synthego ICE web tool (ice.synthego.com). Absence of ATM protein was confirmed by immunoblotting.

Immunoblotting

Following media removal and a PBS wash, cell lysis was performed on 6mm dishes using 50mM Tris HCl plus 2% SDS, with phosphatase and protease inhibitors (Roche#04906837001, Roche#04693159001). Cells were scraped and boiled at 95 °C for 5 minutes, before NanoDrop™ 8000 (A280) protein quantification. Proteins were resolved using the SDS-PAGE gel system (Life Technologies), detected using IRDye secondary antibodies (LI-COR) and visualised on the Odyssey CLx imaging system (LI-COR). Primary antibodies used were obtained from Abcam (ab) or Cell Signaling Technology (CST), unless otherwise stated: ATM (ab78), p-ATM-Ser1981 (ab81292), DNA-PKcs (ab44815), P-DNA-PKcs-Ser2056 (ab18192), KAP1 (ab22553), P-KAP1-Ser824 (ab133440), RPA32 (ab2175), RAD50 (ab89), p-Chk2-Thr68 (ab3501), Chk2 (CST3440), p-Rad50-Ser635 (CST14223S), Chk1 (CST2360), p-Chk1-Ser345 (CST2348), H2AX (CST7631), β-Actin (CST4970), β-Tubulin (CST2146), Lamin B1 (CST12586), Vinculin (CST13901), ATR (Santa Cruz Biotechnology#SC-1887), p-ATR-Thr1989 (Genetex#GTX128145), γH2AX-Ser139 (Millipore#05-636), p-RPA32-Ser4/8 (Bethyl#A300-245A).

Drug sensitivity assays

SRB assays, clonogenic assays and IncuCyte time lapse imaging experiments were performed as we have described previously [4].

Flow cytometry

Cells were plated in a Corning 60mm dishes 24-hours prior to drug treatment. After treatment, cells were trypsinised, fixed with ice-cold 70% EtOH overnight at -20°C, washed, then resuspended in 0.5mL of blocking solution (BS) (PBS, 2% BSA, 0.1% Tween-20, 0.1% Triton X100) for 1 hour. Finally, cells were treated with 0.5mL FxCycle Violet Stain (Invitrogen #F10347), in BS at 1:1000 dilution, and run on the BD Biosciences LSRFortessa™ flow cytometer. The resulting data was analysed using FlowJo® V10 software.

Quantitative image-based cytometry

Cells were seeded in Corning black flat-bottom 96-well plates 24-hours before drug treatment. After treatment, cells were fixed with 4% paraformaldehyde for 10 minutes, permeabilised with 0.1% Triton X-100, 0.1% Tween-20, 1xPBS (PBSTT) for 10 minutes at room temperature and blocked for 30 minutes with BS (same as Flow). Primary antibody in BS was added for 1 hour at room temperature (mouse anti-yH2AX S139, Millipore #05-636, 1:2000 and rabbit anti-phospho-RPA32 S4/8, Bethyl#A300-245A, 1:1000), After washing, secondary antibody (Alexa Fluor 488 goat anti-rabbit, Invitrogen#A11034, 1:500 and Alexa Fluor 568 goat anti-mouse, Invitrogen#A11019, 1:500) plus Hoechst 33342 (Invitrogen#H3570, 1:10,000) in BS was added for 1 hour at room temperature. After washing, images were acquired using the Operetta CLS High-Content Analysis System and analysis performed using Harmony 4.5 software.

Fractionation

Fractionation, to derive cytoplasmic and nuclear fractions, was performed as described by Warren and Eastman in 2019 [24].

Animal experiments

All mouse experiments were carried out in the CRUK-CI BRU, in accordance with the UK Animals (Scientific Procedures) Act 1986, with approval from the CRUK-CI Animal Welfare and Ethical Review Body. Subcutaneous xenografts of MIA PaCa-2 cells were formed by implanting $5x10^6$ cells (in 0.2ml 1:1 matrigel: PBS) in the flank of 7-9-week old female NSG mice (Charles River, 5 mice per cage). Despite some limitations (lack of intra-tumoural heterogeneity, absence of immune responses, reduced ability to recapitulate the tumour microenvironment)

subcutaneous xenografts can offer some advantages over orthotopic models, as previously reported [25], including ease of use, reproducibility and earlier tumour detection. Mice with established tumours (average 242mm^3) were randomised into treatment groups using the 'spiral' randomisation method (see supplement). AZD6738 (AstraZeneca) was dissolved to 5mg/mL in 10% DMSO, 40% Propylene Glycol, 50% de-ionised sterile water and given at 50mg/kg by oral gavage. Gemcitabine (LKT Laboratories, from Cambridge Bioscience) was dissolved in sterile saline (Vetivex) to 10mg/mL and given at 50mg/kg intraperitoneally. Tumours were measured twice a week using callipers. Tumour growth inhibition = [MeanVolCtrl– MeanVolTreated/ MeanVolCtrl] x 100. At endpoint, blood was collected by cardiac puncture (under terminal anaesthesia using isoflurane in accordance with NC3R guidelines) and run on the Mythic 18 haematology analyser as per instructions (Woodley). Mice were killed by cervical dislocation, confirmed by cutting the femoral artery.

Immunohistochemistry

Formalin-fixed, paraffin-embedded sections were immunostained after heat-induced epitope retrieval by sodium citrate at 100°C for 10-20 minutes, using Bond Polymer Refine Detection kit on the automated Bond system according to manufacturer's instructions (Leica). Slides were mounted using Leica CV5030 Coverslipper Workstation and scanned using a ScanScopeXT (Aperio Technologies). Quantification was performed using Halo software (Indica Labs). yH2AX S139 primary antibodies: CST9718 on human xenograft tissues and ab195190 on mouse intestine.

RESULTS

Pharmacological inhibition of ATM sensitises to ATR inhibition in PDAC cell lines

To assess the degree of sensitisation to ATR inhibition associated with loss of ATM function in PDAC cells, we used the selective and potent ATM kinase inhibitor, AZD0156 [26,27], in combination with ATR inhibitor AZD6738 [28]. First, to confirm target engagement, we assessed the ability of AZD0156 to prevent ATM activation in PDAC cells. 6 Gy irradiation (IR) with analysis of P-ATM-S1981 at 0.5-1hr has previously been used by other groups to study ATM activation in human cancer cells [27,29–31]. In MIA PaCa-2, low nanomolar concentrations of

AZD0156 (≥10 nM) successfully abrogated IR-induced ATM auto-phosphorylation (Fig. 1A). In the absence of extrinsic damage, AZD0156 exposure had minimal effect on human or mouse PDAC cell growth when used at concentrations ≤100 nM (Fig. 1B), at which off-target activity is minimised. We next evaluated the degree of growth inhibition induced by AZD6738 (ATRi) across a range of AZD0156 (ATMi) concentrations. 30 nM ATMi sensitised all 6 of the human (Fig. 1C) and mouse (Fig. 1D) PDAC lines tested, to ATR inhibition. Calculation of Loewe synergy scores using Combenefit software [32] showed that the ATRi/ATMi combination synergistically inhibited growth in all 6 of these lines, albeit modestly in the ATRi-resistant PANC-1 (GI_{50} > 30 μM) (Fig. S1). To assess the long-term proliferation capacity of cells exposed to a 24-hour pulse of AZD6738, we then performed clonogenic assays. In this assay, ATMi strikingly sensitised MIA PaCa-2 to ATRi (Fig. 1E).

ATM protein depletion by siRNA knockdown does not sensitise PDAC cells to ATR inhibition

Having identified that pharmacological inhibition of ATM in PDAC cell lines can sensitise to ATRi, we next evaluated the potential for siRNA knockdown of ATM to confer ATRi sensitivity in three human cell lines – MIA PaCa-2, HPAF-II and PANC-1. Despite achieving durable ATM knockdown (88% mean knockdown efficiency across the 3 lines, SD± 7%) (Fig. 2A), this did not significantly sensitise any of the 3 cell lines to 72-hour exposure to AZD6738 (Fig. 2B). Due to this disparity between kinase inactivation (ATMi) and protein depletion (siATM), we hypothesised that reduced expression of ATM may be insufficient to sensitise cells to AZD6738.

Deletion of ATM using CRISPR/Cas9 does significantly sensitise PDAC cells to ATR inhibition

Having observed a sensitisation effect with the ATMi, but not with siATM, we next used CRISPR/Cas9 technology to generate ATM knockout (KO) MIA PaCa-2 single cell clones. By Sanger sequencing (Fig. S2A) and immunoblotting, we identified three clones that did not express detectable ATM and showed no phospho-ATM S1981 upon irradiation (Fig. 2C). These three ATM-null clones were 7-fold more sensitive to AZD6738 than wild-type (WT) MIA PaCa-2 cells (mean ATM-null cells GI_{50} = 0.37 μM; mean ATM-positive cells GI_{50} = 2.73 μM) (Fig. 2D, & S2B). As sensitisation occurred upon ATM knock-out, but not knock-down with siRNA, this suggests that complete loss of ATM function, not just depletion, is necessary to sensitise PDAC cells to ATRi monotherapy.

ATM loss of function sensitises to the combination of AZD6738 and gemcitabine

We next tested whether reduced ATM function could sensitise to the combination of AZD6738 and gemcitabine (ATRi/gem). Kinase inhibition of ATM conferred sensitivity to 72-hour ATRi/gem exposure in MIA PaCa-2 (Fig. 3A) but siRNA depletion did not (Fig. 3B). Meanwhile, genetic deletion of ATM caused a 2.6-fold shift in the mean gemcitabine GI_{50} (Fig. S2B & S2C) and made MIA PaCa-2 cells hypersensitive to ATRi/gem (Fig. 3C). This was particularly evident in assays where the ATRi/gem was pulsed for 24-hours with observation of subsequent cell growth by time-lapse imaging. A 24-hour pulse of 500 nM AZD6738 and 10 nM gemcitabine had no effect on the growth ability of the WT line (growth as percentage of solvent control = 96% +/-7) but maintained durable growth inhibition for at least 4 days in the ATM-KO cells (growth as percentage of solvent control = 7% +/-1) (Fig. 3D & 3E), with a parallel increase in cell death, quantified by YoYo-3 staining (Fig. 3D). The impressive sensitivity of the isogenic ATM-KO cells to the combination of AZD6738 and gemcitabine, provides evidence that complete ATM-loss could be a predictive biomarker of response to ATRi/gem in patients with PDAC.

ATRi/gem-induced DDR activation persists in the absence of ATM function, due to DNA-PK activity

Having found that targeting ATM, by either pharmacological inhibition or by genetic deletion, can sensitise PDAC cells to the combination of AZD6738 and gemcitabine, we next investigated the DDR signalling pathways activated by ATRi/gem, in the presence or absence of ATM function. 24 hour exposure of MIA PaCa-2 cells to 2000 nM ATRi and 30 nM gemcitabine (concentrations known to be synergistic in this line [4]) induced phosphorylation of ATM and its downstream targets RAD50, KAP1 and Chk2 (Fig. 4A). Perhaps paradoxically (since they are reported to be ATM targets), phospho-ATM S1981, phospho-KAP1 S824 and phospho-Chk2 T68 all persisted, even in the presence of ATMi (AZD0156) (Fig 4A). This persistence was specific to ATRi/gem, since irradiation-induced activation of these markers was prevented by 10 nM ATMi (Fig 4A & 1A). This is similar to our previously findings, when we found that the ATRi/gem combination induced P-Chk2 and P-KAP1 to a similar extent in siATM cells as in siCTRL cells [4]. Here, in the ATRi/gem treated samples, we did observe ATMi dose-dependent abrogation of phospho-RAD50 S635 (Fig 4A), a biomarker of ATM activity [33,34], suggesting that the ATMi was acting on-target. Therefore, the persistence of phospho-

Chk2 T68 and others could be due to the activity of another kinase, the most likely candidate being DNA-PK. Indeed, in both MIA PaCa-2 (Fig. 4B) and HPAF-II (Fig. 4C), the phospho-KAP1 and phospho-Chk2 induced by ATRi or ATRi/gem treatment was abrogated by the selective DNA-PK inhibitor, AZD7648 [35]. Along with phospho-ATM, these phosphorylations were only fully prevented upon combined ATMi and DNA-PKi. We also probed for ATR and its downstream partner Chk1. Gemcitabine-induced phospho-ATR T1989 persisted in the presence of ATRi due to ATM-dependent phosphorylation (Fig. 4B). Meanwhile, phospho-Chk1 S345 was only abrogated upon DNA-PK inhibition (Fig. 4B & 4C). Thus, we revealed that much of the downstream DDR activation induced by ATRi or ATRi/gem was not prevented by ATMi (besides phospho-RAD50 and phospho-ATR), because of phosphorylation by DNA-PK.

We next interrogated DDR pathway activation in ATM-KO MIA PaCa-2 cells. Once again, ATRi/gem treatment upregulated phospho-Chk2, phospho-KAP1 and phospho-Chk1 in both the presence and the absence of ATM function (Fig. 4D). These phosphorylations were DNA-PK driven, as evidenced by their abrogation by AZD7648 (Fig. 4D). The low baseline levels of phospho-RAD50 S635 in untreated ATM-KO MIA PaCa-2 cells appeared to be ATR-dependent, consistent with recent findings that in ATM-deficient models ATR can phosphorylate RAD50 [34]. Unlike with Chk2 and KAP1, the ability for the ATM-KO cells to upregulate phospho-RAD50 S635 upon ATRi/gem was significantly impaired in comparison to ATM-WT. The modest phospho-RAD50 S635 that was induced by ATRi/gem was DNA-PK-dependent (Fig. 4D). Meanwhile, phosphorylation of ATR T1989 appeared to be ATR- and ATM-dependent but not DNA-PK-dependent (Fig. 4D).

Despite the contribution of DNA-PK to many of the DDR phosphorylations in ATRi-treated cells, Bliss and Loewe cytotoxicity synergy scores showed consistently less synergy for the AZD6738 and AZD7648 (DNAPKi) combination than for AZD6738 and AZD0156 (ATMi) across human and mouse PDAC cell lines (Fig 4E, 4F & Fig.S3A). Furthermore, in triple combination SRB experiments, the addition of DNAPKi to ATRi/gem led to only moderate sensitisation compared to ATMi (Fig 4G, 4H & Fig.S3D). This suggests that ATM function is more critical to cell survival during ATRi or ATRi/gem exposure than DNA-PK activity. It also implies that the Chk1/Chk2 phosphorylations that arise through DNA-PK activity do not play a major protective role in ATRi/gem-exposed PDAC cells.

ATRi/gem-induced replication catastrophe is augmented in ATM-null PDAC cells

We next investigated the effect of AZD6738 and gemcitabine treatment on the cell cycle profile of ATM-proficient and ATM-deficient PDAC cells. Treatment with 500 nM AZD6738 and 10 nM gemcitabine for 24 hours had little-to-no effect on the cell cycle profile of WT MIA PaCa-2 cells. Conversely, 10 nM gemcitabine induced significant intra-S accumulation in the ATM-KO MIA PaCa-2, along with a reduction in the G2-M proportion (Fig 5A). This was augmented by the addition of 500 nM AZD6738, which also increased the sub-G1 fraction, indicating induction of cell death. When the higher concentration of 2000 nM AZD6738 was used, we observed modest intra-S accumulation with ATRi-monotherapy, which was specific to the ATM-null cells, while addition of 30 nM gemcitabine could induce S-phase arrest in both the ATM-WT and ATM-KO cells (Fig. S4A).

Through immunoblotting we had found that ATRi/gem treatment induced DNA-PK-driven activation of the checkpoint proteins, Chk1 and Chk2. However, co-treating with the DNA-PKi AZD7648 did not alter the cell cycle profiles in any of the ATRi/gem conditions (Fig. S4A), indicating that the intra-S phase arrests we observed were independent of checkpoint activation. An alternative reason for the intra-S accumulation, independent of a checkpoint, could be induction of replication catastrophe. This is defined as the widespread breakage of multiple replication forks, resulting from a global exhaustion of RPA and subsequent degradation of unprotected ssDNA at stalled forks [7,24,36]. We found that 500 nM AZD6738 and 10 nM gemcitabine caused RPA32 to deplete from the cytosol and accumulate in the nucleus over time, with a parallel increase in nuclear yH2AX S139, in the ATM-KO MIA PaCa-2 (Fig 5B). Next, using quantitative image-based cytometry, we assessed the degree of replication catastrophe induced by ATRi and ATRi/gem in ATM-WT vs ATM-KO, by quantifying the emergence of cells with pan-nuclear yH2AX S139 and pan-nuclear phospho-RPA32 S4/8 (Fig 5C & S4B). After 24–hour exposure to 500 nM AZD6738 alone, just 1.4% of WT MIA PaCa-2 cells were pan-nuclear for both markers, compared to 8.7% of ATM-KO cells (Fig 5D). The combination of 500 nM AZD6738 and 10 nM gemcitabine induced pan-nuclear yH2AX S139 and phospho-RPA32 in both cell types, but much more extensively in the ATM-KO cells (9.9% WT double-positive vs 58.2% ATM-KO double-positive after 24 hours) (Fig 5E). Hoechst quantification confirmed that the majority of the cells with pan-nuclear damage had DNA contents between 2n and 4n, consistent with S-phase failure (Fig. S4C). Our observation of

increased replication catastrophe in the ATM-KO cells suggests that ATM protects against nuclear-wide fork collapse during ATRi/gem treatment.

AZD6738 monotherapy causes growth delay in ATM-deficient PDAC xenografts, while combined treatment with gemcitabine induces regression

Next, we assessed the efficacy of AZD6738 monotherapy *in vivo*. We treated NSG mice bearing either MIA PaCa-2 WT or MIA PaCa-2 ATM-KO subcutaneous xenografts, with 50 mg/kg AZD6738 (oral gavage, once daily, 5 consecutive days a week) for three weeks. No efficacy was seen in the ATM-proficient model, whereas in the ATM-KO tumours we observed a 61% tumour growth inhibition (TGI) after 3 weeks of treatment (Fig. 6A). Subsequently, we assessed whether we could use low dose gemcitabine as a sensitiser to AZD6738, to perhaps improve on the already impressive response seen with ATRi alone in the ATM-KO model. Regression is rare in MIA PaCa-2 xenograft studies, but adding gemcitabine (50 mg/kg, IP, once per week) to the 50 mg/kg AZD6738 schedule induced regression in the ATM-KO MIA PaCa-2 tumours (mean volume change after 3 weeks = -17.8%, 95% confidence interval -2.7% to -32.8%), and growth delay in the WT tumours (46% TGI) (Fig. 6B & S5A). As expected with this xenograft model, no metastases were identified in any group. The dose-schedules used were well tolerated such that, across the two studies, just two mice experienced notable weight loss - one in the gemcitabine-alone group (1/17) and one in ATRi/gem group (1/17) (Fig. S5B). Endpoint blood cell counts showed no significant difference between the ATRi/gem combination group and gemcitabine single agent (Fig. S5C).

IHC quantification of yH2AX percent positive nuclei in the tumours, fixed 6 hours after the final dose, revealed an increase in the ATRi/gem groups compared to vehicle; mean yH2AX positivity increased from 5.7% to 11.4% in WT tumours with ATRi/gem ($p < 0.01$), and from 7.3% to 15.4% in ATM-KO tumours with ATRi/gem compared to vehicle ($p <0.0001$) (Fig. 6D & Fig. S5D). yH2AX positivity was higher in the ATM-KO tumours following ATRi/gem treatment compared to the ATM-WT ($p<0.05$). In both sets of tumours, the yH2AX positivity persisted for at least 24 hours after dosing (Fig. 6D). Meanwhile in the small intestine, the high yH2AX induced at 6 hours by gemcitabine or ATRi/gem did not persist (Fig. 6E), indicative of DNA repair in normal tissue.

DISCUSSION

The application of precision medicine strategies, where therapies are assigned based on patient-specific tumour vulnerabilities, has the potential to improve outcomes for diseases such as PDAC. Having launched a phase I trial to assess the combination of AZD6738 and gemcitabine (ATRiUM, NCT03669601), we sought to investigate the potential utility of ATM-loss as a predictive biomarker of response for ATRi/gem in PDAC. ATM and ATR have been reported to share a synthetic lethal relationship in some cancer types [17–19,37,38]. However, it has become increasingly clear that most synthetic lethal interactions depend highly on the genetic background in which they are studied [39]. By targeting ATM through multiple methods, our data indicate that complete loss of ATM function is necessary to sensitise PDAC cells to AZD6738 or the AZD6738 and gemcitabine combination. This has important implications, as it brings into question how best to assess ATM status in future clinical trials.

A recent example of a trial where ATM status was assessed is Study 39 (NCT01063517). This was a phase II efficacy study assessing the combination of olaparib and paclitaxel in gastric cancer patients, which identified a greater overall survival benefit in patients with "ATM-low" tumours [40]. Here, "ATM-low" tumours were defined as those with ≤10% ATM tumour cell nuclear staining, quantified by an IHC test using the ATM (Y170) antibody clone. In the follow-up phase III GOLD trial (NCT01924533), a new IHC reporter assay was developed that used the same antibody clone but with different assay configurations and reagents [41]. The cut-off for "ATM-low" tumours was redefined as <25% of ATM tumour cell nuclear staining (to account for increased sensitivity of new assay) however this trial failed to meet its primary endpoint and failed to confirm the survival benefit in "ATM-low" patients that had been observed previously [42]. It remains unclear whether redefining the cut-off to a lower threshold would bring a different result. In relation to ATRi/gem in PDAC, our data would support the use of complete ATM-loss (i.e. 0% ATM tumour cell nuclear staining), as opposed to <10 or 25% staining, since only ATM-null cells appeared to be hypersensitive. This leads to the question of how to identify ATM-null tumours in a clinical setting. Such tumour samples have been identified previously, including in the very first phase I dose escalation trial of an ATR inhibitor, which identified a colorectal cancer patient with 100% ATM loss by IHC, who showed a complete response (19+ months) to M660 monotherapy [43,44]. Evaluating ATM functionality by IHC, using markers such as phospho-ATM and phospho-RAD50 [34], in

conjunction with total ATM could add further depth to ATM status assessments, however this would likely require patients to be challenged with an DSB-inducing agent prior to biopsy to be most informative. The presence of germline or somatic ATM mutations, combined with a low IHC score, would add confidence that a patient's tumour is indeed ATM negative, thus incorporating next-generation sequencing (NGS) in parallel with IHC could improve clinical biomarker assessments [45]. On the whole, if precision medicine techniques are to be implemented successfully, it is becoming increasingly apparent that the field will have to be more precise and detailed in the characterisation of patients and their tumours, and multi-modal assessments of patient samples may facilitate this.

As well as the important distinction between ATM-low and ATM-null, our data also reveal further insight into the mechanism of how AZD6738 and gemcitabine synergise to induce cell death. The increase in nuclear RPA over time upon ATRi/gem exposure, plus the accumulation of S-phase cells pan-nuclear for DNA damage and replication stress markers, suggests that the combination induces replication catastrophe (RC) (Fig. 5). During this catastrophic fork collapse, Chk1 and Chk2 are phosphorylated by DNA-PK, but the lack of clear ATRi/DNAPKi synergy and the inability for DNA-PKi to significantly potentiate ATRi/gem (Fig 4G), suggests that these DNA-PK-driven signals may be bystander events during RC. The fact that ATM-deficient cells are hypersensitive to ATRi/gem-induced RC indicates that ATM plays a critical role in protecting against this widespread fork collapse. A recent study found that topotecan- or olaparib-induced breakage of replication forks is lethal in ATM-deficient models due to the induction of toxic non-homologous end joining (NHEJ) [23]. Their data suggested that the toxic NHEJ was mediated by XRCC4 and ligase IV, but not DNA-PK. Here, we found that DNA-PKi did not significantly potentiate nor attenuate the effect of ATRi/gem in WT or ATM-KO cells. Going forward, it will be interesting to interrogate whether the hypersensitivity of ATM-null PDAC cells to ATRi/gem is also due to toxic NHEJ.

Minimising toxicity is a major challenge when combining DDRi and chemotherapy in the clinic. Most phase I trials of this type are designed such that the DNA-damaging cytotoxic is administered at its standard-of-care dose – i.e. at the expected maximum tolerated dose – and the DDRi is titrated in at increasing levels. As a result, any increase in toxicity will immediately become dose limiting and the true potential of these combinations may not be fully explored. The ATRiUM trial design is unique, in that it is using a model-based approach

to guide dose escalation, starting each drug at dosages that are <100% of the predicted or actual single agent dose. In essence, the aim is to use the gemcitabine as a sensitiser to the AZD6738, rather than simply administering the cytotoxic at its typical maximum dosage. In the pre-clinical study reported here, we demonstrated that this strategy can indeed be effective, particularly in an ATM-deficient setting. We first found that 50 mg/kg AZD6738 monotherapy, once daily for 5 consecutive days a week, induced significant growth delay in the ATM-null tumours. Rather than introduce gemcitabine at its typical pre-clinical single agent dose of 100 mg/kg twice per week [46], we used a comparatively low gemcitabine dose of 50 mg/kg, once per week, to allow pharmacodynamically effective dose schedules of AZD6738. This regimen induced growth delay in the ATM-WT and tumour regression in the ATM-KO tumours (Fig 6B), thus demonstrating proof-of-principle that low dose gemcitabine can be used as a sensitiser to AZD6738 *in vivo*.

As well as assessing the safety, tolerability and preliminary anti-tumour activity of ATRi/gem in a novel model-based approach, the ATRiUM trial is incorporating IHC assessment of baseline ATM, NGS of patient DNA and on-treatment biopsies. This will enable some of the conclusions we have made in this study to be scrutinised clinically. This could steer the design of future precision-medicine based trials that will examine the promise that ATM shows as a predictive biomarker of response for AZD6738 and gemcitabine combination therapy in PDAC.

ADDITIONAL INFORMATION

Acknowledgments

We would like to thank the Core Facilities at the Cancer Research UK Cambridge Institute, including the Biological Resources Unit, Research Instrumentation & Cell Services, Histopathology, Light Microscopy and Flow Cytometry for technical provision, as well as members of the Pharmacology & Drug Development Group for discussions. Thanks to Professor Stephen Jackson of the Wellcome Trust/CRUK Gurdon Institute, Cambridge, for providing the pAiO-WT-ATM plasmid. Thanks to AstraZeneca for provision of AZD6738, AZD0156 and AZD7648.

Authors' contributions

Investigation, CRD; Additional support in data acquisition, YW, TIJ, SBQ;

Provision of compound and guidance in compound usage, STD, EBC, AL;
Writing-Original Draft Preparation, CRD; Writing-Review & Editing, CRD, FMR, DIJ;
Supervision, FMR, YW, DIJ.

Ethical approval

All mouse experiments were carried out in the CRUK-CI BRU, in accordance with the UK Animals (Scientific Procedures) Act 1986, with approval from the CRUK-CI Animal Welfare and Ethical Review Body.

Consent to publish

All authors have granted consent for publication of the data shown

Data availability

All original data is archived and stored at the Cancer Research UK Cambridge Institute, Cambridge, UK. Cell lines generated in this study - MIA PaCa-2 ATM-KO (clones B4, B7, C4) and controls - will be made available to other researchers upon request.

Competing interests

YW, STD, EBC, AL are employees of AstraZeneca. TIJ recently became an employee of Artios Pharma. DIJ has received research funding from AstraZeneca for both laboratory research and clinical trial projects.

Funding

CRD, YW, TIJ, SBQF, FMR and DIJ were funded by Cancer Research UK Institute core grants C14303/A17197 and C9545/A29580. *In vivo* studies were funded by Cancer Research UK Precision Panc grant C96/A25238. CRD was also a recipient of funding from the Pancreatic Cancer UK Future Research Leaders Fund grant RG81962. The Li Ka Shing Centre in which this research was performed was generously funded by CK Hutchison Holdings Limited, the University of Cambridge, Cancer Research UK, The Atlantic Philanthropies and a range of other projects.

REFERENCES

1 Siegel, R.L., Miller, K.D., Jemal, A. Cancer statistics, 2020. CA Cancer J Clin 70, 7–30 (2020)

2 Vincent, A., Herman, J., Schulick, R., Hruban, R.H., Goggins, M. Pancreatic cancer. Lancet Lond Engl 378, 607–620 (2011)

3 Conroy, T., Desseigne, F., Ychou, M., Bouché, O., Guimbaud, R., Bécouarn, Y. et al. FOLFIRINOX versus gemcitabine for metastatic pancreatic cancer. N Engl J Med 364, 1817–1825 (2011)

4 Wallez, Y., Dunlop, C.R., Johnson, T.I., Koh, S-B., Fornari, C., Yates, J.W.T. et al. The ATR Inhibitor AZD6738 Synergizes with Gemcitabine In Vitro and In Vivo to Induce Pancreatic Ductal Adenocarcinoma Regression. Mol Cancer Ther 17, 1670–1682 (2018)

5 Iyer, D.R., Rhind, N. The Intra-S Checkpoint Responses to DNA Damage. Genes 8, 74 (2017)

6 Zeman, M.K., Cimprich, K.A. Causes and consequences of replication stress. Nat Cell Biol 16, 2–9 (2014)

7 Toledo, L.I., Altmeyer, M., Rask, M-B., Lukas, C., Larsen, D.H., Povlsen, L.K. et al. ATR Prohibits Replication Catastrophe by Preventing Global Exhaustion of RPA. Cell 155, 1088–1103 (2013)

8 Sanchez, Y., Wong, C., Thoma, R.S., Richman, R., Wu, Z., Piwnica-Worms, H. et al. Conservation of the Chk1 Checkpoint Pathway in Mammals: Linkage of DNA Damage to Cdk Regulation Through Cdc25. Science 277, 1497–1501 (1997)

9 Sørensen, C.S., Syljuåsen, R.G., Falck, J., Schroeder, T., Rönnstrand, L., Khanna, K.K. et al. Chk1 regulates the S phase checkpoint by coupling the physiological turnover and ionizing radiation-induced accelerated proteolysis of Cdc25A. Cancer Cell 3, 247–258 (2003)

10 Mini, E., Nobili, S., Caciagli, B., Landini, I., Mazzei, T. Cellular pharmacology of gemcitabine. Ann Oncol Off J Eur Soc Med Oncol ESMO 17 Suppl 5, v7-12 (2006)

11 Banin, S., Moyal, L., Shieh, S-Y., Taya, Y., Anderson, C.W., Chessa L. et al. Enhanced Phosphorylation of p53 by ATM in Response to DNA Damage. Science 281, 1674–1677 (1998)

12 Canman, C.E., Lim, D-S., Cimprich, K.A., Taya, Y., Tamai, K., Sakaguchi, K. et al. Activation of the ATM Kinase by Ionizing Radiation and Phosphorylation of p53. Science 281, 1677–1679 (1998)

13 Roberts, N.J., Jiao, Y., Yu, J., Kopelovich, L., Petersen, G.M., Bondy, M.L. et al. ATM mutations in patients with hereditary pancreatic cancer. Cancer Discov 2, 41–46 (2012)

14 Armstrong, S.A., Schultz, C.W., Azimi-Sadjadi, A., Brody, J.R., Pishvaian, M.J. ATM Dysfunction in Pancreatic Adenocarcinoma and Associated Therapeutic Implications. Mol Cancer Ther 18, 1899–1908 (2019)

15 Kamphues, C., Bova, R., Bahra, M., Klauschen, F., Muckenhuber, A., Sinn, B.V. et al. Ataxia-telangiectasia-mutated protein kinase levels stratify patients with pancreatic adenocarcinoma into prognostic subgroups with loss being a strong indicator of poor survival. Pancreas 44, 296–301 (2015)

16 Kim, H., Saka, B., Knight, S., Borges, M., Childs, E., Klein, A. et al. Having pancreatic cancer with tumoral loss of ATM and normal TP53 protein expression is associated with a poorer prognosis. Clin Cancer Res Off J Am Assoc Cancer Res 20, 1865–1872 (2014)

17 Kwok, M., Davies, N., Agathanggelou, A., Smith, E., Oldreive, C., Petermann, E. et al. ATR inhibition induces synthetic lethality and overcomes chemoresistance in TP53- or ATM-defective chronic lymphocytic leukemia cells. Blood 127, 582–595 (2016)

18 Min, A., Im, S-A., Jang, H., Kim, S., Lee, M., Kim, D.K. et al. AZD6738, A Novel Oral Inhibitor of ATR, Induces Synthetic Lethality with ATM Deficiency in Gastric Cancer Cells. Mol Cancer Ther 16, 566–577 (2017)

19 Vendetti, F.P., Lau, A., Schamus, S., Conrads, T.P., O'Connor, M.J., Bakkenist, C.J. The orally active and bioavailable ATR kinase inhibitor AZD6738 potentiates the anti-tumor effects of cisplatin to resolve ATM-deficient non-small cell lung cancer in vivo. Oncotarget 6, 44289–44305 (2015)

20 Ayars, M., Eshleman, J., Goggins, M. Susceptibility of ATM-deficient pancreatic cancer cells to radiation. Cell Cycle 16, 991–998 (2017)

21 Perkhofer, L., Schmitt, A., Romero Carrasco, M.C., Ihle, M., Hampp, S., Ruess, D.A. et al. ATM Deficiency Generating Genomic Instability Sensitizes Pancreatic Ductal Adenocarcinoma Cells to Therapy-Induced DNA Damage. Cancer Res 77, 5576–5590 (2017)

22 Olive, K.P., Jacobetz, M.A., Davidson, C.J., Gopinathan, A., McIntyre, D., Honess, D. et al. Inhibition of Hedgehog Signaling Enhances Delivery of Chemotherapy in a Mouse Model of Pancreatic Cancer. Science 324, 1457–1461 (2009)

23 Balmus, G., Pilger, D., Coates, J., Demir, M., Sczaniecka-Clift, M., Barros, A.C. et al. ATM orchestrates the DNA-damage response to counter toxic non-homologous end-joining at broken replication forks. Nat Commun 10, 87 (2019)

24 Warren, N.J.H., Eastman, A. Inhibition of checkpoint kinase 1 following gemcitabine-mediated S phase arrest results in CDC7- and CDK2-dependent replication catastrophe. J Biol Chem 294, 1763–1778 (2019)

25 Dorado, M.R-M., Gómez, L.M.M., Sánchez, D.A., Arenas, S.P., Praena-Fernández, J.M., Martín, J.J.B. et al. Translational pancreatic cancer research: A comparative study on patient-derived xenograft models. World J Gastroenterol 24, 794–809 (2018)

26 Barlaam, B., Pike, K. Identifying high quality, potent and selective inhibitors of ATM kinase: Discovery of AZD0156. Eur J Cancer 61, S118–S118 (2016)

27 Pike, K.G., Barlaam, B., Cadogan, E., Campbell, A., Chen, Y., Colclough, N. et al. The Identification of Potent, Selective, and Orally Available Inhibitors of Ataxia Telangiectasia Mutated (ATM) Kinase: The Discovery of AZD0156 (8-{6-[3-(Dimethylamino)propoxy]pyridin-3-yl}-3-methyl-1-(tetrahydro-2H- pyran-4-yl)-1,3-dihydro-2H-imidazo[4,5-c]quinolin-2-one). J Med Chem 61, 3823–3841 (2018)

28 Foote, K.M., Nissink, J.W.M., McGuire, T., Turner, P., Guichard, S., Yates, J.W.T. et al. Discovery and Characterization of AZD6738, a Potent Inhibitor of Ataxia Telangiectasia Mutated and Rad3 Related (ATR) Kinase with Application as an Anticancer Agent. J Med Chem 61, 9889–9907 (2018)

29 Hoey, C., Ray, J., Jeon, J., Huang, X., Taeb, S., Ylanko, J. et al. miRNA-106a and prostate cancer radioresistance: a novel role for LITAF in ATM regulation. Mol Oncol 12, 1324–1341 (2018)

30 Lee, H-J., Yoon, C., Schmidt, B., Park, D.J., Zhang, A.Y., Erkizan, H.V. et al. Combining PARP-1 Inhibition and Radiation in Ewing Sarcoma Results in Lethal DNA Damage. Mol Cancer Ther 12, 2591–2600 (2013)

31 Park, S-Y., Kim, Y.M., Pyo, H. Gefitinib radiosensitizes non-small cell lung cancer cells through inhibition of ataxia telangiectasia mutated. Mol Cancer 9 222 (2010)

32 Di Veroli, G.Y., Fornari, C., Wang, D., Mollard, S., Bramhall, J.L., Richards, F.M. et al. Combenefit: an interactive platform for the analysis and visualization of drug combinations. Bioinforma Oxf Engl 32 2866–2868 (2016)

33 Gatei, M., Jakob, B., Chen, P., Kijas, A.W., Becherel, O.J., Gueven, N. et al. ATM protein-dependent phosphorylation of Rad50 protein regulates DNA repair and cell cycle control. J Biol Chem 286, 31542–31556 (2011)

34 Jones, G.N., Rooney, C., Griffin, N., Roudier, M., Young, L.A., Garcia-Trinidad, A. et al. pRAD50: a novel and clinically applicable pharmacodynamic biomarker of both ATM and ATR inhibition identified using mass spectrometry and immunohistochemistry. Br J Cancer 119, 1233–1243 (2018)

35 Fok, J.H.L., Ramos-Montoya, A., Vazquez-Chantada, M., Wijnhoven, P.W.G., Follia, V., James, N. et al. AZD7648 is a potent and selective DNA-PK inhibitor that enhances radiation, chemotherapy and olaparib activity. Nat Commun 10, 1–15 (2019)

36 Toledo, L., Neelsen, K.J., Lukas, J. Replication Catastrophe: When a Checkpoint Fails because of Exhaustion. Mol Cell 66, 735–749 (2017)

37 Schmitt, A., Knittel, G., Welcker, D., Yang, T-P., George, J., Nowak, M. et al. ATM Deficiency Is Associated with Sensitivity to PARP1-and ATR Inhibitors in Lung Adenocarcinoma. Cancer Res 77, 3040–3056 (2017)

38 Jette, N.R., Radhamani, S., Arthur, G., Ye, R., Goutam, S., Bolyos, A. et al. Combined poly-ADP ribose polymerase and ataxia-telangiectasia mutated/Rad3-related inhibition targets ataxia-telangiectasia mutated-deficient lung cancer cells. Br J Cancer 121, 600–610 (2019)

39 Ryan, C.J., Bajrami, I., Lord, C.J. Synthetic Lethality and Cancer - Penetrance as the Major Barrier. Trends Cancer 4, 671–683 (2018)

40 Bang, Y-J., Im, S-A., Lee, K-W., Cho, J.Y., Song, E-K., Lee, K.H. et al. Randomized, Double-Blind Phase II Trial With Prospective Classification by ATM Protein Level to Evaluate the Efficacy and Tolerability of Olaparib Plus Paclitaxel in Patients With Recurrent or Metastatic Gastric Cancer. J Clin Oncol Off J Am Soc Clin Oncol 33, 3858–3865 (2015)

41 Miller, R.M., Nworu, C., McKee, L., Balcerzak, D., Pham, L., Pugh, J. et al. Development of an Immunohistochemical Assay to Detect the Ataxia-Telangiectasia Mutated (ATM) Protein in Gastric Carcinoma. Appl Immunohistochem Mol Morphol 28, 303–310 (2020)

42 Bang, Y-J., Xu, R-H., Chin, K., Lee, K-W., Park, S.H., Rha, S.Y. et al. Olaparib in combination with paclitaxel in patients with advanced gastric cancer who have progressed following first-line therapy (GOLD): a double-blind, randomised, placebo-controlled, phase 3 trial. Lancet Oncol 18, 1637–1651 (2017)

43 O'Carrigan, B., de Miguel Luken, M.J., Papadatos-Pastos, D., Brown, J., Tunariu, N., Perez Lopez, R. et al. Phase I trial of a first-in-class ATR inhibitor VX-970 as monotherapy (mono) or in combination (combo) with carboplatin (CP) incorporating pharmacodynamics (PD) studies. J Clin Oncol 34, 2504–2504 (2016)

44 Yap, T.A., de Miguel Luken, M.J., O'Carrigan, B., Roda, D., Papadatos-Pastos, D., Lorente, D. et al. Abstract PR14: Phase I trial of first-in-class ataxia telangiectasia-mutated and Rad3-related (ATR) inhibitor VX-970 as monotherapy (mono) or in combination with carboplatin (CP) in advanced cancer patients (pts) with preliminary evidence of target modulation and antitumor activity. Mol Cancer Ther 14, PR14–PR14 (2015)

45 Sundar, R., Miranda, S., Rodrigues, D.N., Chénard-Poirier, M., Dolling, D., Clarke, M. et al. Ataxia Telangiectasia Mutated Protein Loss and Benefit From Oxaliplatin-based Chemotherapy in Colorectal Cancer. Clin Colorectal Cancer 17, 280–284 (2018)

46 Bapiro, T.E., Frese, K.K., Courtin, A., Bramhall, J.L., Madhu, B., Cook, N. et al. Gemcitabine diphosphate choline is a major metabolite linked to the Kennedy pathway in pancreatic cancer models in vivo. Br J Cancer 111, 318–325 (2014)

FIGURE LEGENDS

Figure 1. Pharmacological inhibition of ATM sensitises to ATR inhibition in PDAC cell lines

A. MIA PaCa-2 were incubated with AZD0156 for 1 hour before exposure to 6 Gy of y-irradiation (IR). 30 mins post-IR, cells were harvested for immunoblot analysis. **B.** Human and mouse cell lines were exposed to AZD0156 for 72 hours to generate dose-response curves using the SRB assay. Each point represents the mean of three independent experiments ± SEM. **C-D.** AZD6738 dose response curve with and without 30 nM AZD0156, mean ± SEM, n=3, with GI_{50} plus 95% confidence intervals shown. Human (C) and mouse (D) lines were treated for 72 hours. **E.** Clonogenic survival of MIA PaCa-2 cells plated at low density and exposed to the indicated drug combinations for 24 hours before washout. Cells were left to grow for 7 days after washout. Each point represents the mean of three independent experiments ± SEM. The difference between *AZD6738* and *AZD6738 + 30 nM ATMi* was assessed using multiple t-tests. * indicates $p \leq 0.05$, ** $p \leq 0.01$.

Figure 2. Deletion of ATM using CRISPR/Cas9, but not protein depletion by siRNA knockdown, sensitises PDAC cells to ATR inhibition

A. ATM protein expression in human cell lines at the start (T0) of the drug sensitivity assay (48 hours post-transfection) and at the 72-hour assay endpoint (120 hours post-transfection). Two different "exposures" of the ATM blot are shown (by adjusting brightness of the IRDye image in LiCor Image Studio). Percentage knockdown values versus siCTR are displayed, derived using LiCor Image Studio quantification software. **B.** AZD6738 dose-response curves of human lines, having been transfected with either a non-targeting siRNA control pool (siCTR) or with an ATM-targeting siRNA pool (siATM). Assay duration was 72-hours. Each point represents the mean of three independent experiments ± SEM. **C.** 30 mins post 6 Gy of y-irradiation (IR), MIA PaCa-2 single cell clones from a CRISPR/Cas9 ATM knockout pool were harvested for immunoblot analysis to determine the ATM status. Clones B4, B7 and C4 were confirmed ATM-null. **D.** AZD6738 dose-response curves of MIA PaCa-2 CRISPR clones. Assay duration was 72-hours. Each point represents the mean of three independent experiments ± SEM.

Figure 3. ATM loss of function sensitises to the combination of AZD6738 and gemcitabine

A. The effect of ATM kinase inhibition by AZD0156 on ATRi (AZD6738) and gemcitabine sensitivity in MIA PaCa-2. **B.** The effect of ATM depletion by siRNA on AZD6738 & gemcitabine sensitivity in MIA PaCa-2**. C.** The effect of ATM deletion by CRISPR/Cas9 on AZD6738 & gemcitabine sensitivity in MIA PaCa-2. In all three panels (A-C), MIA PaCa-2 in the conditions listed were treated with increasing concentrations of AZD6738 and gemcitabine for 72 hours. Left = Matrices display growth as % of solvent control (as assessed by SRB assay), mean ± SD, n=3. Right = AZD6738 dose response curves in the presence of 1 nM or 10 nM gemcitabine, mean ± SEM, n=3. **D.** MIA PaCa-2 WT and MIA PaCa-2 ATM-KO (clone B7) cells in medium containing the YOYO-3 Iodide cell-impermeant dye were treated with AZD6738 and gemcitabine in a 6 × 8 concentration grid for 24 hours (grey bar denotes period of drug treatment). The drugs were washed out and replaced with fresh YOYO-3-containing medium. Three fields per sample were imaged by IncuCyte time lapse microscopy every 3 hours for 4

days post-washout. Phase Object Confluence was quantified as the percentage of the image area occupied by cells (left). Cell death accumulation (right) was quantified by measuring Red Object Confluence, and expressed as a percentage of the total Object Confluence. Each curve is a representative of three independent experiments. **E.** The same cells from the IncuCyte experiment in (D) were fixed in TCA 4 days post-washout and the relative growth was assessed by SRB assay. Left = growth as % of solvent control, mean ± SD, n=3 independent experiments. Right = Combenefit synergy score (Loewe).

Figure 4. ATRi/gem-induced DDR activation persists in the absence of ATM function, due to DNA-PK activity

A. Immunoblot analysis of MIA PaCa-2 cells. Cells which received 6 Gy of y-irradiation (IR) were harvested 30 mins post-IR. All other samples were harvested after 24 hours of drug exposure. ATRi + GEM denotes 2 µM AZD6738 and 30 nM gemcitabine. ATMi is AZD0156 and was either applied concurrently with ATRi/gem, or administered one hour prior to IR, in the case of the two IR samples. **B.** Immunoblot analysis of MIA PaCa-2 cells. Cells were harvested after 24 hours of drug exposure. ATRi is AZD6738, ATMi is AZD0156, DNA-PKi is AZD7648. **C.** Immunoblot analysis of HPAF-II cells. Cells were harvested after 24 hours of drug exposure. **D.** Immunoblot analysis of MIA PaCa-2 WT and MIA PaCa-2 ATM-KO cells (clone B7). Cells were harvested after 24 hours of drug exposure. **E.** Cells were treated with increasing concentrations of ATRi (AZD6738) & DNA-PKi (AZD7648) for 72 hours and growth was assessed by SRB assay. Top = growth as % of solvent control. Bottom = Combenefit synergy score (Loewe). Data, mean ± SD, n=3. For matrices of all cell lines see Fig S2. **F**. Synergy comparison of the AZD6738 & AZD0156 combination (ATRi + ATMi, see Fig. 1C & 1D) vs the AZD6738 & AZD7648 combination (ATRi + DNAPKi). Cells were treated with increasing concentrations for 72 hours and growth as % of solvent control was assessed by SRB assay. Combenefit software was used to calculate the sum of synergy and antagonism across the dose ranges tested. **G.** The effect of DNA-PK inhibition on AZD6783 & gemcitabine sensitivity in MIA PaCa-2. Values denote growth as % of solvent control (as assessed by SRB assay), mean ± SD, n=3. **H.** Visualisation of how much more effect ATM inhibition has compared to DNA-PK inhibition, on the growth of ATRi/gem-treated MIAPaCa-2. Left = the *%Control* values of the *MIA PaCa-2 + 1 µM DNA-PKi* matrix from Fig. 4G were subtracted from those of the *MIA PaCa-2 + DMSO* matrix from Fig. 4G. Right = the *%Control* values of the *MIA PaCa-2 + 30 nM ATMi* matrix from Fig. 3A were subtracted from those of the *MIA PaCa-2 + DMSO* matrix from Fig. 3A.

Figure 5. ATRi/gem-induced replication catastrophe is augmented in ATM-null PDAC cells

A. DNA content of MIA PaCa-2 WT and MIA PaCa-2 ATM-KO (clone B7) cells following 24-hour exposure of the indicated drugs. Left = Representative DNA content histograms, x = FxCycle Violet fluorescence (DNA content), y = cell count. Right = cell cycle distribution. Each bar represents the mean of 3 independent experiments ± SD. A one-way ANOVA analysis, comparing the % S phase fractions, was performed with Tukey's multiple comparisons tests, * indicates $p \leq 0.05$, ** $p \leq 0.01$, *** $p \leq 0.001$. **B.** Immunoblot analysis of MIA PaCa-2 WT and MIA PaCa-2 ATM-KO cells treated as indicated, separated by cytosolic and nuclear fractions. **C.** Representative images showing the pan-nuclear emergence of yH2AX S139 and phospho-

RPA32 S4/8 upon 24-hour exposure to 500 nM AZD6738 and 10 nM gemcitabine. The images shown were acquired using a 10x objective lens. Images acquired using a 20x objective lens are displayed in Fig. S4B. **D-E.** Quantitative image-based cytometry to determine the proportion of cells pan-nuclear for both yH2AX S139 and phospho-RPA32 S4/8, at the timepoints indicated. ATRi = 500 nM AZD6738. GEM = 10 nM gemcitabine. Images were acquired using the Operetta CLS High-Content Analysis System (10x objective) and analysis performed using Harmony 4.5 software. The resulting data were imported into FlowJo as CSV files to generate the pseudo-colour plots shown. Percentages of double-positive cells are shown.

Figure 6. AZD6738 monotherapy causes growth delay in ATM-deficient PDAC xenografts, while combined treatment with gemcitabine induces regression

A. Tumour volumes of MIA PaCa-2 WT and MIA PaCa-2 ATM-KO (clone B7) xenografts in NSG mice, with AZD6738 monotherapy at 50 mg/kg, OG, once daily, 5 days on & 2 days off. Grey bars denote the 5-day dosing cycles. Data, mean ± SEM. WT-Vehicle group, n=10. WT-AZD6738 group, n=9. ATM KO-Vehicle group, n=9. ATM KO-AZD6738 group, n=9. **B.** AZD6738 and gemcitabine combination. AZD6738 was given at 50 mg/kg, OG, once daily, 5 days on & 2 days off. Gemcitabine was given at 50 mg/kg, IP, once per week on day 1 of each dosing cycle. Grey bars denote the 5-day dosing cycles. MIA PaCa-2 WT-Vehicle group, n=8. WT-Gemcitabine group, n=7. WT-AZD6738 & Gemcitabine group, n = 7. One mouse from the WT-Gemcitabine group and one from the WT-AZD6738 & Gemcitabine group dropped weight in the first week and their tumour volumes are not included in the mean values shown. MIA PaCa-2 ATM KO-Vehicle group, n=8. ATM KO-Gemcitabine group, n=9. ATM KO-AZD6738 group, n=8. ATM KO-AZD6738 & Gemcitabine group, n=9. **C-D** Nuclear yH2AX S139 positivity in the formalin-fixed tumour (C) and small intestine (D) samples from the combination study was assessed by IHC and quantified using Halo software. Each point represents data from one histological section from an individual mouse. Horizontal bars denote the mean. A one-way ANOVA analysis was performed with Tukey's multiple comparisons tests, * indicates $p \leq 0.05$, **$p \leq 0.01$, ***$p \leq 0.001$, ****$p \leq 0.0001$.

Figure 1

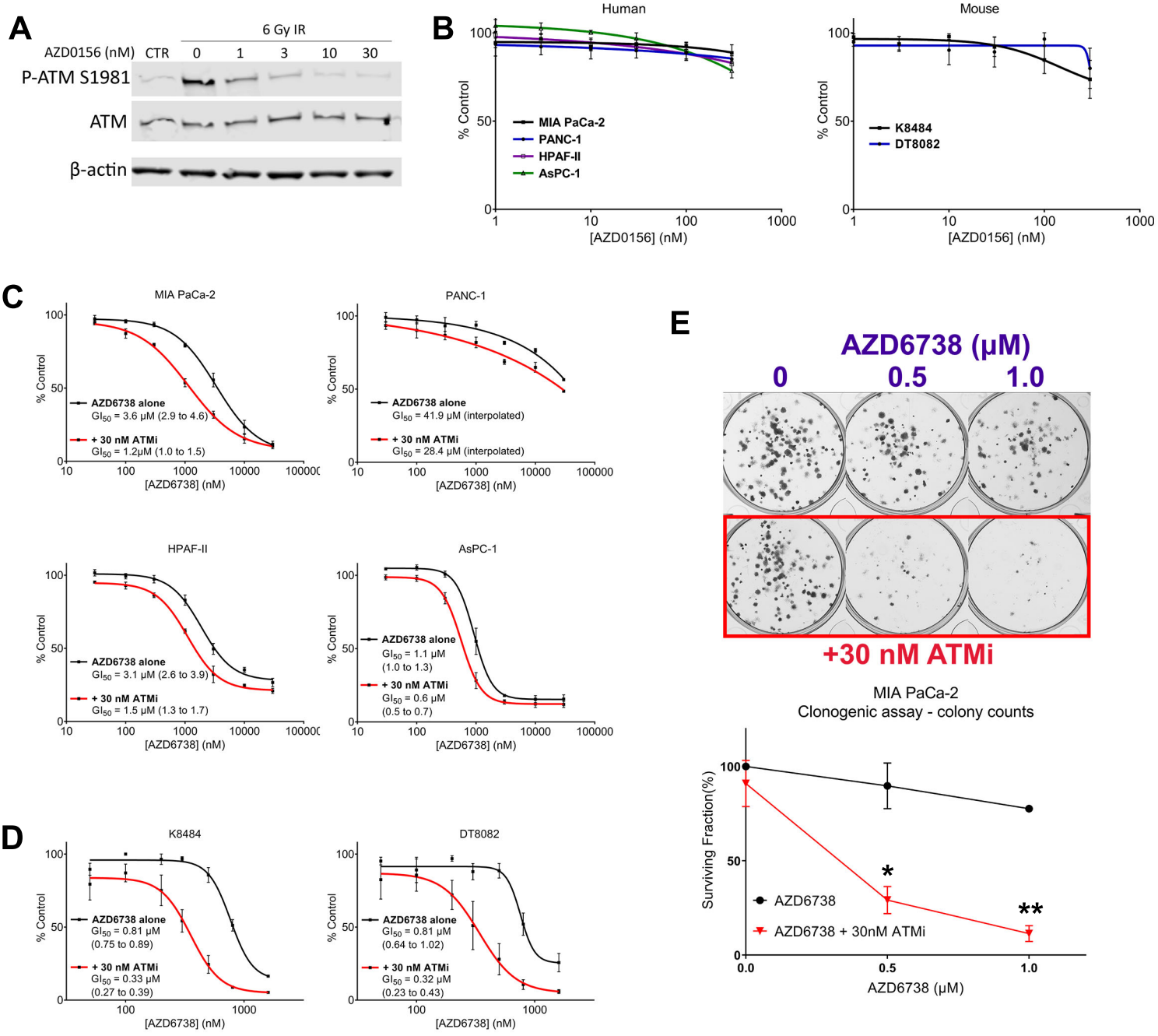
A
6 Gy IR
AZD0156 (nM) CTR 0 1 3 10 30
P-ATM S1981
ATM
β-actin
B
Human
% Control
MIA PaCa-2
PANC-1
HPAF-II
AsPC-1
[AZD0156] (nM)
Mouse
K8484
DT8082
[AZD0156] (nM)
C
MIA PaCa-2
AZD6738 alone
GI50 = 3.6 μM (2.9 to 4.6)
+ 30 nM ATMi
GI50 = 1.2μM (1.0 to 1.5)
[AZD6738] (nM)
PANC-1
AZD6738 alone
GI50 = 41.9 μM (interpolated)
+ 30 nM ATMi
GI50 = 28.4 μM (interpolated)
HPAF-II
AZD6738 alone
GI50 = 3.1 μM (2.6 to 3.9)
+ 30 nM ATMi
GI50 = 1.5 μM (1.3 to 1.7)
AsPC-1
AZD6738 alone
GI50 = 1.1 μM
(1.0 to 1.3)
+ 30 nM ATMi
GI50 = 0.6 μM
(0.5 to 0.7)
D
K8484
AZD6738 alone
GI50 = 0.81 μM
(0.75 to 0.89)
+ 30 nM ATMi
GI50 = 0.33 μM
(0.27 to 0.39)
DT8082
AZD6738 alone
GI50 = 0.81 μM
(0.64 to 1.02)
+ 30 nM ATMi
GI50 = 0.32 μM
(0.23 to 0.43)
E
AZD6738 (μM)
0 0.5 1.0
+30 nM ATMi
MIA PaCa-2
Clonogenic assay - colony counts
Surviving Fraction(%)
AZD6738
AZD6738 + 30nM ATMi
AZD6738 (μM)

Figure 2

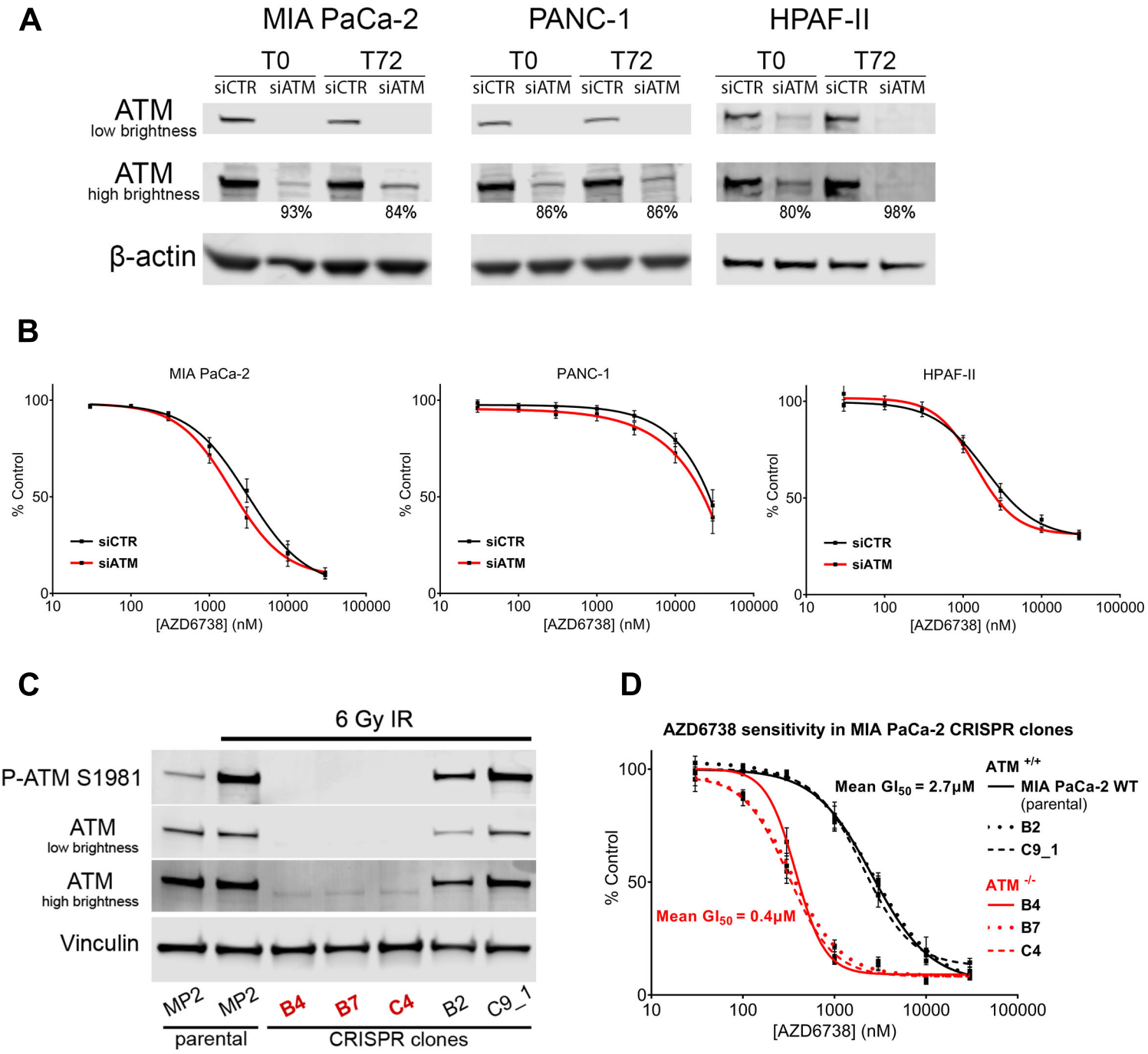
A
MIA PaCa-2
PANC-1
HPAF-II
T0
T72
siCTR siATM siCTR siATM
ATM
low brightness
ATM
high brightness
93%
84%
86%
86%
80%
98%
β-actin
B
MIA PaCa-2
PANC-1
HPAF-II
% Control
siCTR
siATM
[AZD6738] (nM)
C
6 Gy IR
P-ATM S1981
ATM
low brightness
ATM
high brightness
Vinculin
MP2
MP2
B4
B7
C4
B2
C9_1
parental
CRISPR clones
D
AZD6738 sensitivity in MIA PaCa-2 CRISPR clones
Mean GI50 = 2.7μM
Mean GI50 = 0.4μM
ATM +/+
MIA PaCa-2 WT
(parental)
B2
C9_1
ATM -/-
B4
B7
C4
% Control
[AZD6738] (nM)

Figure 3

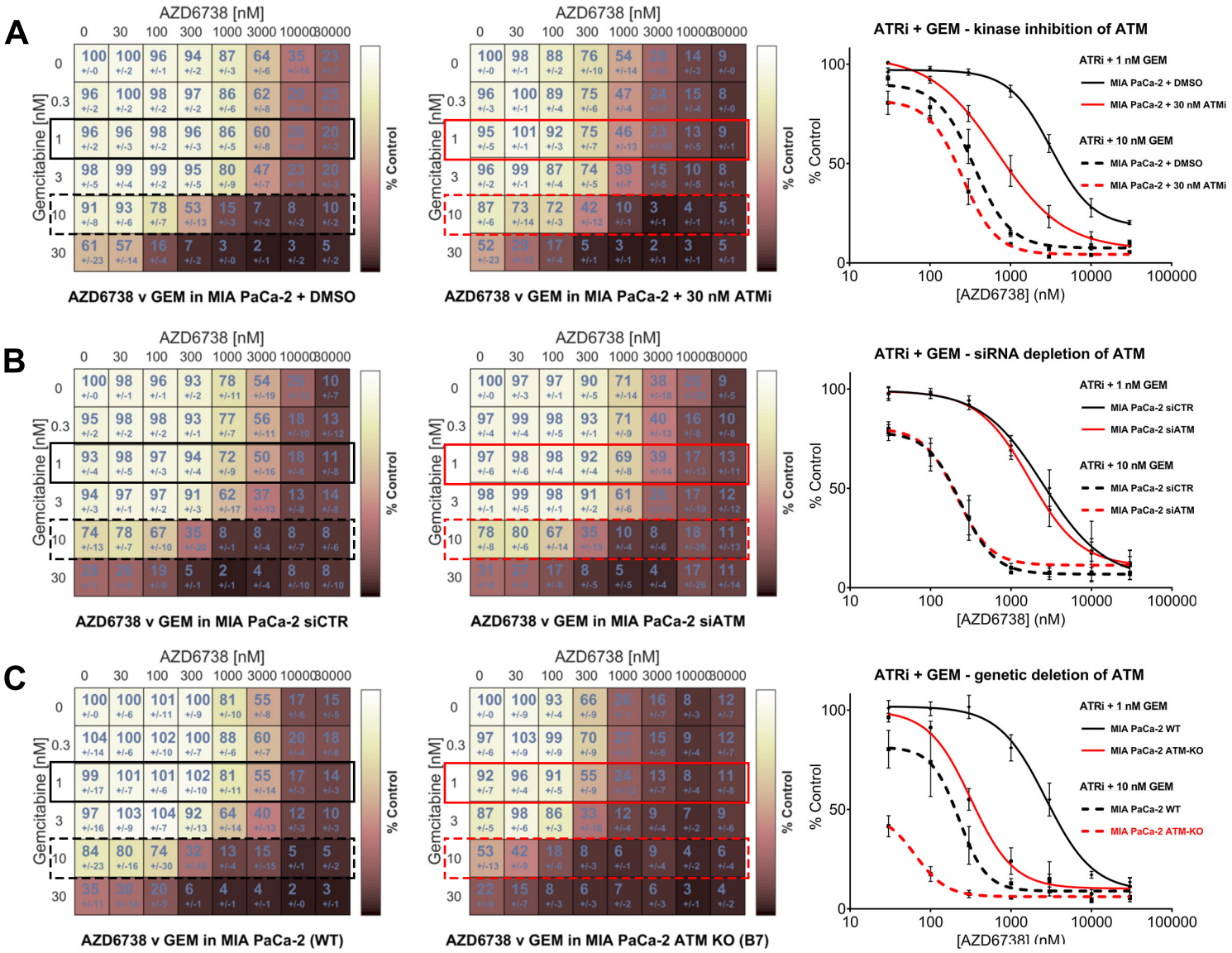
A
AZD6738 [nM]
Gemcitabine [nM]
% Control
AZD6738 v GEM in MIA PaCa-2 + DMSO
AZD6738 v GEM in MIA PaCa-2 + 30 nM ATMi
ATRi + GEM - kinase inhibition of ATM
ATRi + 1 nM GEM
MIA PaCa-2 + DMSO
MIA PaCa-2 + 30 nM ATMi
ATRi + 10 nM GEM
[AZD6738] (nM)
B
AZD6738 v GEM in MIA PaCa-2 siCTR
AZD6738 v GEM in MIA PaCa-2 siATM
ATRi + GEM - siRNA depletion of ATM
MIA PaCa-2 siCTR
MIA PaCa-2 siATM
C
AZD6738 v GEM in MIA PaCa-2 (WT)
AZD6738 v GEM in MIA PaCa-2 ATM KO (B7)
ATRi + GEM - genetic deletion of ATM
MIA PaCa-2 WT
MIA PaCa-2 ATM-KO

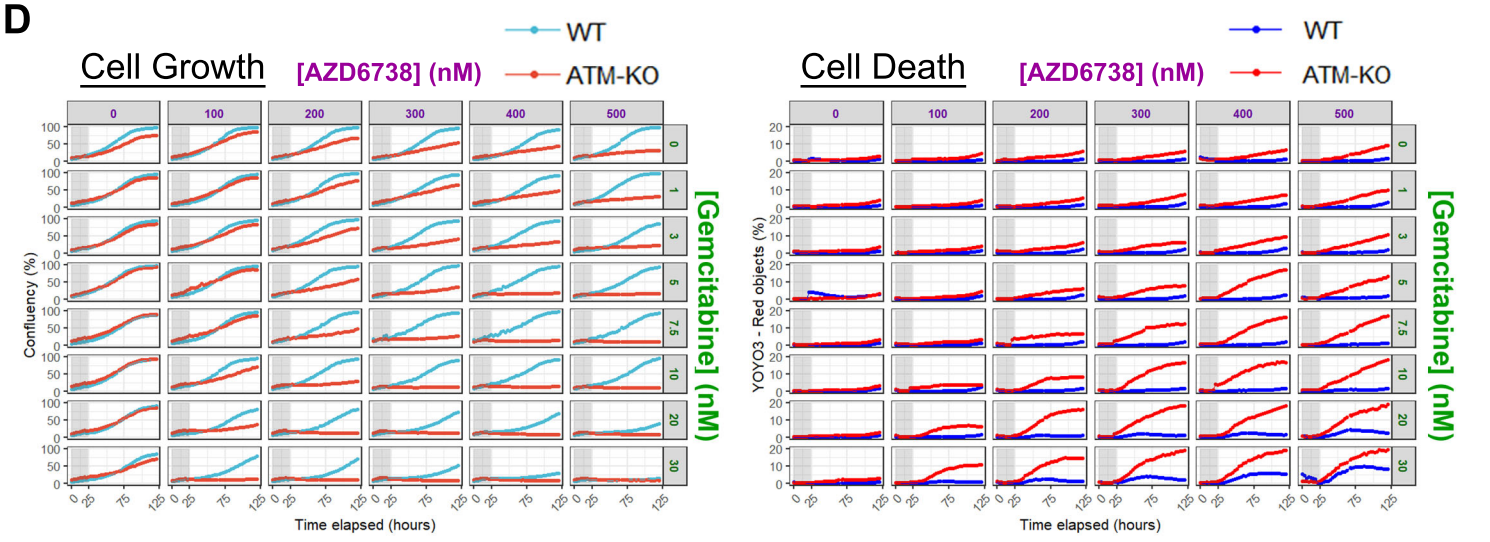
D
Cell Growth
Cell Death
[AZD6738] (nM)
WT
ATM-KO
Confluency (%)
YOYO3 - Red objects (%)
[Gemcitabine] (nM)
Time elapsed (hours)

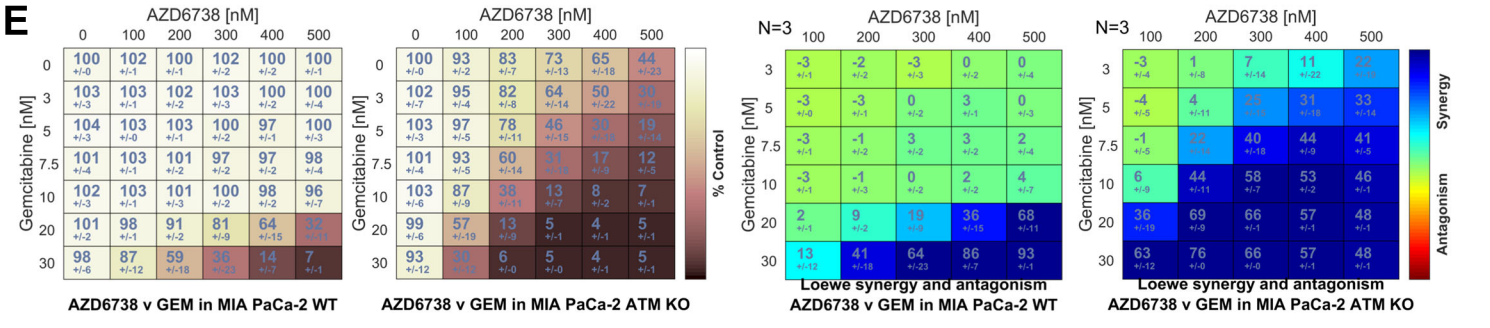
E
AZD6738 [nM]
Gemcitabine [nM]
% Control
N=3
Synergy
Antagonism
AZD6738 v GEM in MIA PaCa-2 WT
AZD6738 v GEM in MIA PaCa-2 ATM KO
Loewe synergy and antagonism
AZD6738 v GEM in MIA PaCa-2 WT
AZD6738 v GEM in MIA PaCa-2 ATM KO

Figure 4

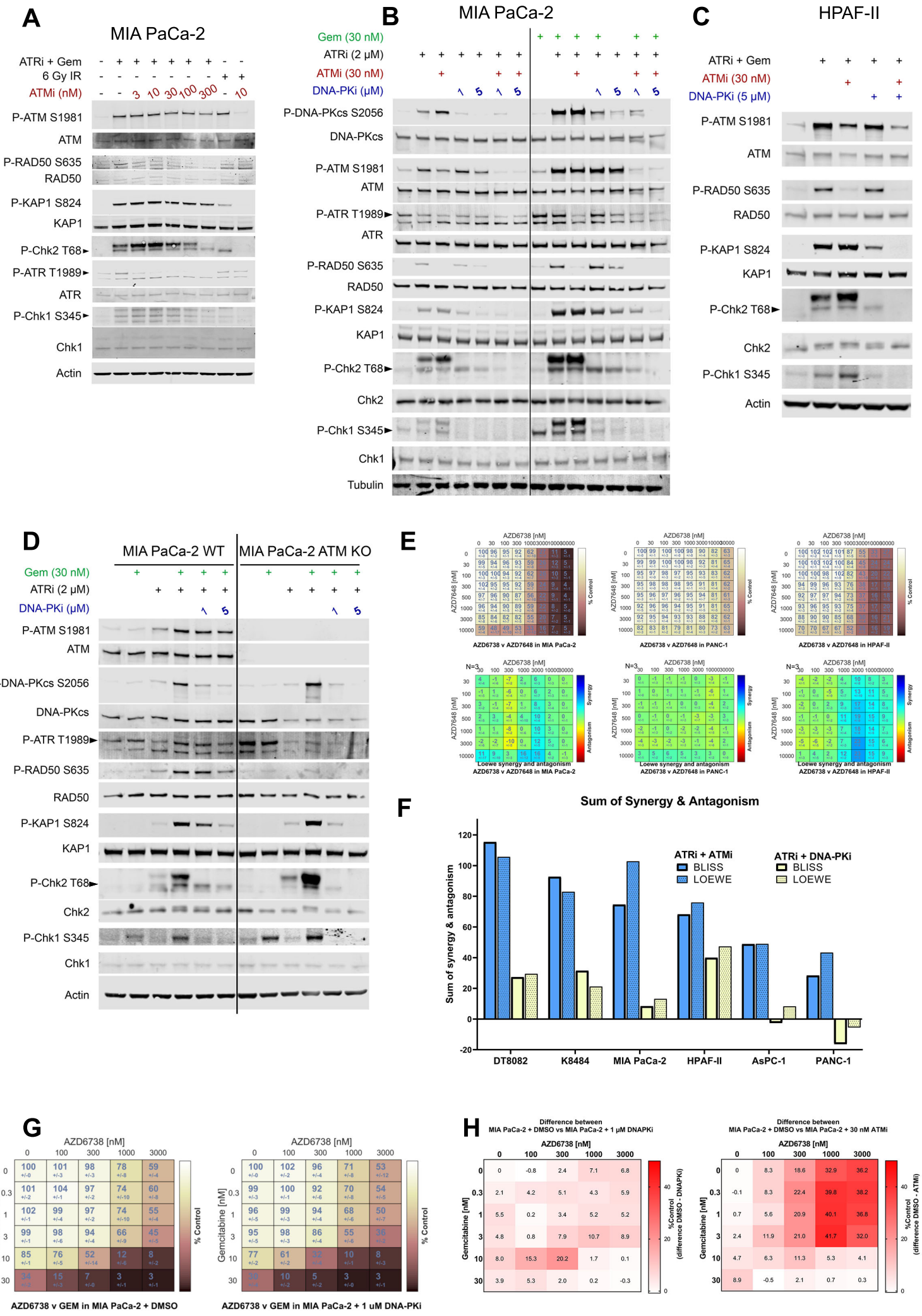
A
MIA PaCa-2
ATRi + Gem
6 Gy IR
ATMi (nM)
P-ATM S1981
ATM
P-RAD50 S635
RAD50
P-KAP1 S824
KAP1
P-Chk2 T68
P-ATR T1989
ATR
P-Chk1 S345
Chk1
Actin
B
MIA PaCa-2
Gem (30 nM)
ATRi (2 μM)
ATMi (30 nM)
DNA-PKi (μM)
P-DNA-PKcs S2056
DNA-PKcs
P-ATM S1981
ATM
P-ATR T1989
ATR
P-RAD50 S635
RAD50
P-KAP1 S824
KAP1
P-Chk2 T68
Chk2
P-Chk1 S345
Chk1
Tubulin
C
HPAF-II
ATRi + Gem
ATMi (30 nM)
DNA-PKi (5 μM)
P-ATM S1981
ATM
P-RAD50 S635
RAD50
P-KAP1 S824
KAP1
P-Chk2 T68
Chk2
P-Chk1 S345
Actin
D
MIA PaCa-2 WT
MIA PaCa-2 ATM KO
Gem (30 nM)
ATRi (2 μM)
DNA-PKi (μM)
P-ATM S1981
ATM
P-DNA-PKcs S2056
DNA-PKcs
P-ATR T1989
P-RAD50 S635
RAD50
P-KAP1 S824
KAP1
P-Chk2 T68
Chk2
P-Chk1 S345
Chk1
Actin
E
AZD6738 [nM]
% Control
AZD6738 v AZD7648 in MIA PaCa-2
AZD6738 v AZD7648 in PANC-1
AZD6738 v AZD7648 in HPAF-II
N=3
Synergy
Antagonism
Loewe synergy and antagonism
F
Sum of Synergy & Antagonism
Sum of synergy & antagonism
ATRi + ATMi
BLISS
LOEWE
ATRi + DNA-PKi
BLISS
LOEWE
DT8082
K8484
MIA PaCa-2
HPAF-II
AsPC-1
PANC-1
G
AZD6738 [nM]
Gemcitabine [nM]
% Control
AZD6738 v GEM in MIA PaCa-2 + DMSO
AZD6738 v GEM in MIA PaCa-2 + 1 uM DNA-PKi
H
Difference between
MIA PaCa-2 + DMSO vs MIA PaCa-2 + 1 μM DNAPKi
AZD6738 [nM]
Gemcitabine [nM]
%Control (difference DMSO - DNAPKi)
Difference between
MIA PaCa-2 + DMSO vs MIA PaCa-2 + 30 nM ATMi
AZD6738 [nM]
Gemcitabine [nM]
%Control (difference DMSO - ATMi)

Figure 5

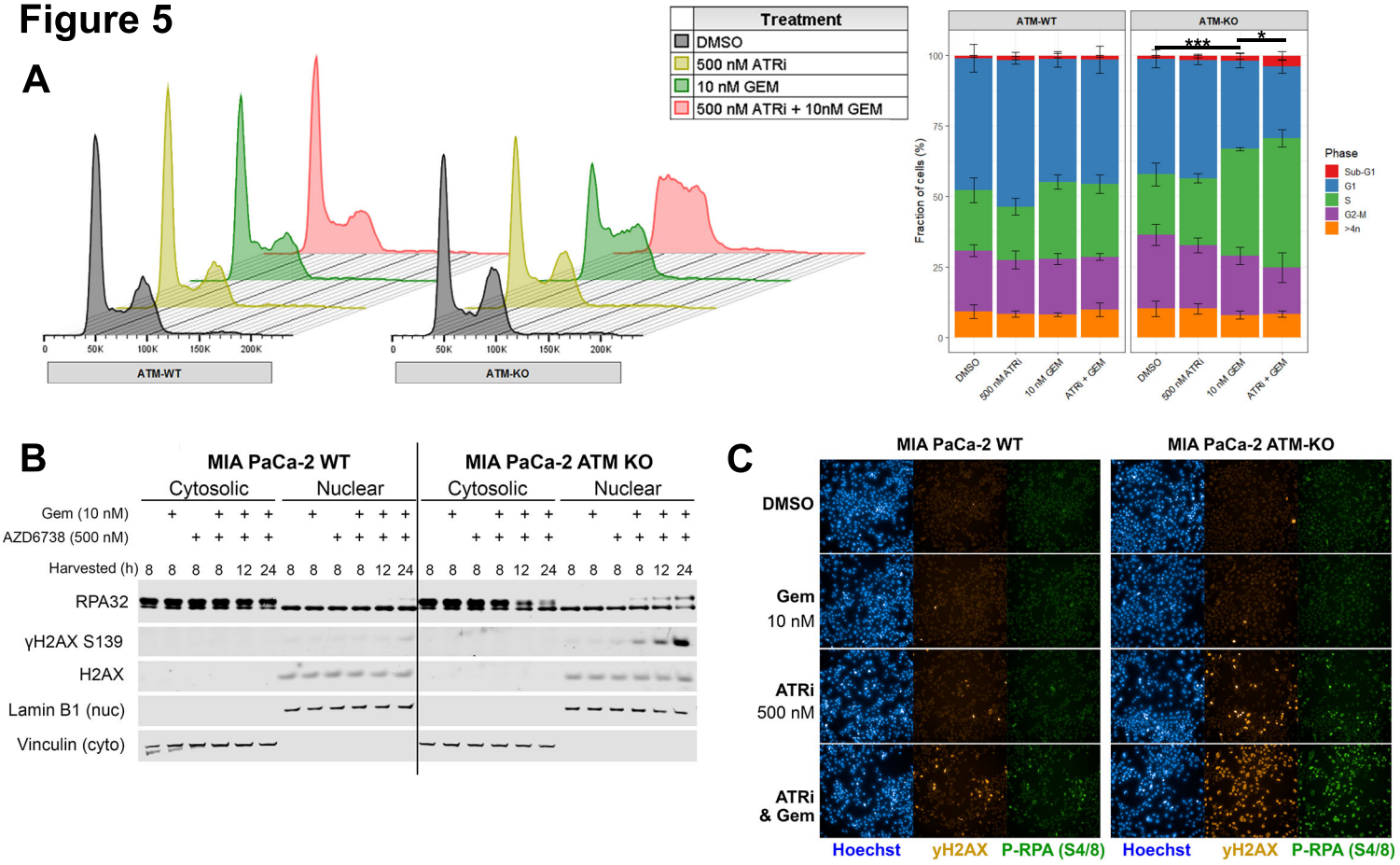
A
Treatment
DMSO
500 nM ATRi
10 nM GEM
500 nM ATRi + 10nM GEM
ATM-WT
ATM-KO
Fraction of cells (%)
Phase
Sub-G1
G1
S
G2-M
>4n
DMSO
500 nM ATRi
10 nM GEM
ATRi + GEM
B
MIA PaCa-2 WT
MIA PaCa-2 ATM KO
Cytosolic
Nuclear
Gem (10 nM)
AZD6738 (500 nM)
Harvested (h)
RPA32
γH2AX S139
H2AX
Lamin B1 (nuc)
Vinculin (cyto)
C
MIA PaCa-2 WT
MIA PaCa-2 ATM-KO
DMSO
Gem 10 nM
ATRi 500 nM
ATRi & Gem
Hoechst
γH2AX
P-RPA (S4/8)
D
WT
KO
DMSO
ATRi 8hr
ATRi 12hr
ATRi 24hr
0.3%
1.1%
1.4%
1.4%
0.5%
4.9%
5.9%
8.7%
γH2AX (Alexa-568)
pRPA S4/8 (Alexa-488)
E
WT
KO
DMSO
ATRi+GEM 8hr
ATRi+GEM 12hr
ATRi+GEM 24hr
0.3%
2.1%
4.6%
9.9%
0.5%
15.4%
28.7%
58.2%

Figure 6

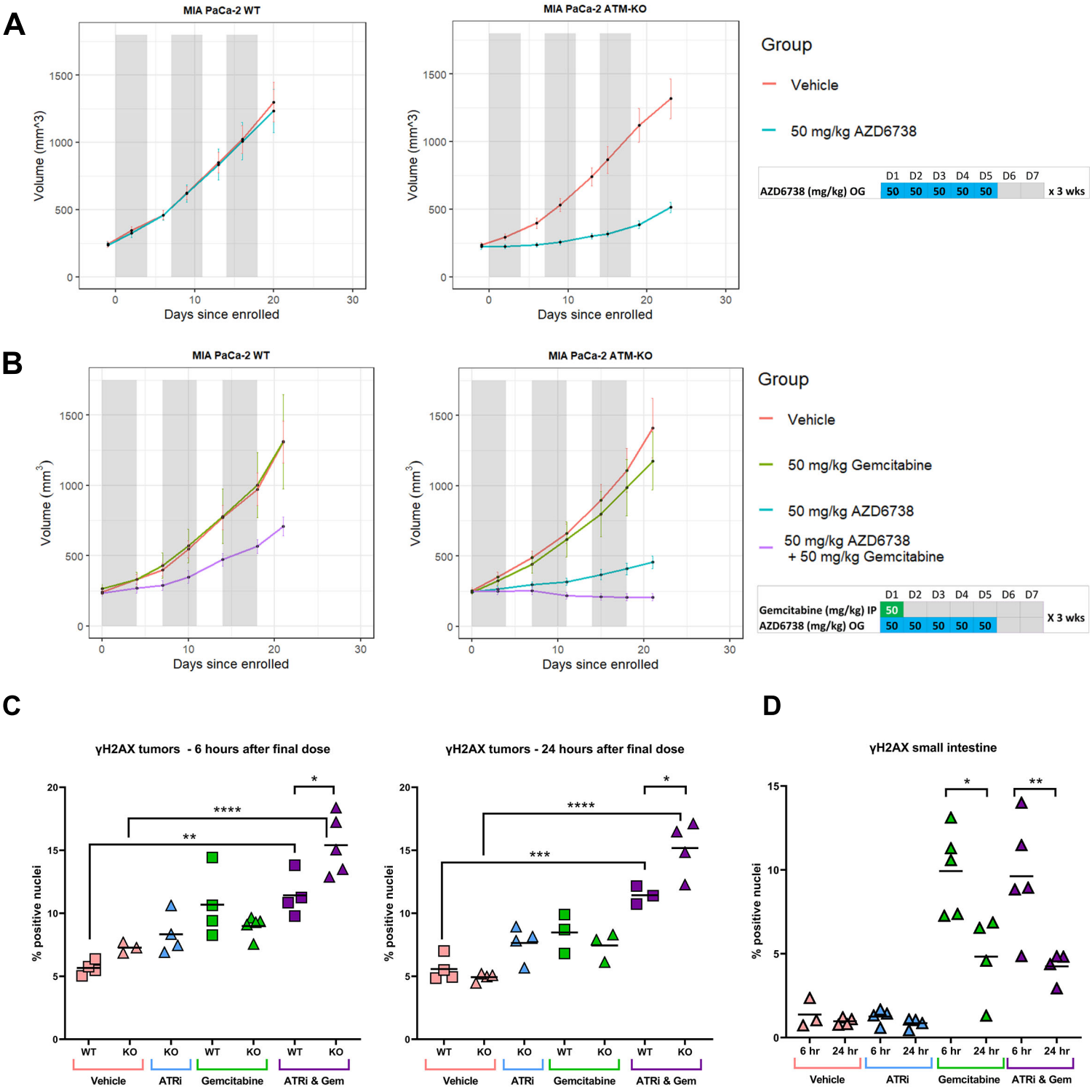
A
MIA PaCa-2 WT
MIA PaCa-2 ATM-KO
Volume (mm^3)
Days since enrolled
Group
Vehicle
50 mg/kg AZD6738
D1 D2 D3 D4 D5 D6 D7
AZD6738 (mg/kg) OG
50 50 50 50 50
x 3 wks
B
MIA PaCa-2 WT
MIA PaCa-2 ATM-KO
Volume (mm3)
Days since enrolled
Group
Vehicle
50 mg/kg Gemcitabine
50 mg/kg AZD6738
50 mg/kg AZD6738
+ 50 mg/kg Gemcitabine
D1 D2 D3 D4 D5 D6 D7
Gemcitabine (mg/kg) IP
AZD6738 (mg/kg) OG
50
50 50 50 50 50
X 3 wks
C
γH2AX tumors - 6 hours after final dose
γH2AX tumors - 24 hours after final dose
% positive nuclei
WT KO KO WT KO WT KO
Vehicle ATRi Gemcitabine ATRi & Gem
D
γH2AX small intestine
% positive nuclei
6 hr 24 hr 6 hr 24 hr 6 hr 24 hr 6 hr 24 hr
Vehicle ATRi Gemcitabine ATRi & Gem